phys. stat. sol. (a) **39**, 561 (1977)

Subject classification: 10.1; 11; 21.1

Institut für Physik am Max-Planck-Institut für Metallforschung, Stuttgart

Transmission Electron Microscope Studies of Dislocation Loops in Heavy-Ion Irradiated H.C.P. Cobalt

By

H. FÖLL and M. WILKENS

Thin foils of h.c.p. cobalt are irradiated at room temperature with 60 keV Au ions (dose between 10^{11} and 10^{12} ions/cm^2) and subsequently investigated by TEM. The dislocation loops of vacancy type (mean diameter ≈ 7 nm) produced in the cores of the displacement cascades are analysed with respect to their loop normals $\boldsymbol{n}$ and their Burgers vectors $\boldsymbol{b}$ using for the contrast analysis the first order perturbation method. For most of the loops the analysis yielded $\boldsymbol{b} = a/3\langle 11\bar{2}0\rangle$ and $\boldsymbol{n} \approx \{10\bar{1}0\}$, $\sphericalangle\, \boldsymbol{n}, \boldsymbol{b} \approx 30°$. A small fraction of the loops are found to be of pure edge type with $\boldsymbol{b} = a/2\langle 10\bar{1}0\rangle$, $\boldsymbol{n} = \{10\bar{1}0\}$. The results are interpreted in terms of a model of loop formation which predicts loop configurations in h.c.p. metals depending on the axial ratio c/a. It is shown that the experimental data published in the literature on dislocation loops in radiation damaged or quenched h.c.p. metals are in agreement with the model.

Durchstrahlungspräparate von hexagonal dichtest gepacktem Kobalt werden bei Raumtemperatur mit Goldionen (Energie = 60 keV, Dosis zwischen 10^{11} und 10^{12} Ionen/cm^2) bestrahlt und anschließend im Elektronenmikroskop untersucht. Es werden Versetzungsringe vom Leerstellentyp (mittlerer Durchmesser ≈ 7 nm) gefunden, die in den Zentren der Verlagerungskaskaden entstehen. Die Kontrastanalyse ergibt $\boldsymbol{b} = a/3\langle 11\bar{2}0\rangle$ und $\boldsymbol{n} \approx \{10\bar{1}0\}$, $\sphericalangle\, \boldsymbol{b}, \boldsymbol{n} \approx 30°$ ($\boldsymbol{b}$ = Burgersvektor und $\boldsymbol{n}$ = Normale der Versetzungsringe). Ein kleiner Bruchteil der Ringe hat reinen Stufencharakter mit $\boldsymbol{b} = a/2\langle 10\bar{1}0\rangle$. Die Beobachtungen werden mit einem Modell der Bildung von Versetzungsringen gedeutet, das für hexagonal dicht gepackte Metalle einen Einfluß des Achsenverhältnisses c/a auf die Konfiguration der Versetzungsringe voraussagt. Es wird gezeigt, daß die experimentellen Beobachtungen, die in der Literatur über die Konfiguration von Versetzungsringen in strahlengeschädigten oder abgeschreckten hexagonal dicht gepackten Metallen veröffentlicht sind, mit dem vorgeschlagenen Modell im Einklang stehen.

1. Introduction

Detailed transmission electron microscope (TEM) studies of radiation damage in f.c.c. and b.c.c. metals have shown that the irradiation-produced point defects (vacancies or interstitials) show a strong tendency to agglomerate into dislocation loops. This loop formation occurs — in many cases — in two steps: In a first step the loops are formed as "Frank sessile loops" on the close-packed lattice planes with a partial Burgers vector $\boldsymbol{b}_F$ ($\{111\}$-planes in f.c.c. metals, $\boldsymbol{b}_F = \frac{1}{3}\langle 111\rangle$; $\{110\}$-planes in b.c.c. metals, $\boldsymbol{b}_F = \frac{1}{2}\langle 110\rangle$). In a second step, which is sometimes suppressed, depending on the stacking fault energy, the Frank loops may be converted into configurations of lower total energy, e.g., by a transformation of $\boldsymbol{b}_F$ into a perfect Burgers vector $\boldsymbol{b}_p$ ($\boldsymbol{b}_p = \frac{1}{2}\langle 110\rangle$ in f.c.c. metals, $\boldsymbol{b}_p = \frac{1}{2}\langle 111\rangle$ in b.c.c. metals) or — in the case of f.c.c. metals of low stacking fault energy — into dissociated Frank loops or stacking fault tetrahedra. For reviews, see Wilkens [1 to 3], Eyre [4].

If this concept is applicable also to h.c.p. metals one would expect that in these metals the crystallographic structure of dislocation loops formed by clustering of non-equilibrium point defects (produced by radiation damage or quenching from high temperatures) should depend on the axial ratio c/a: For $c/a > \sqrt{3}$ the close-packed

planes are parallel to {0001} whereas for $c/a < \sqrt{3}$ this holds for the $\{10\bar{1}0\}$ planes. In Section 4.2 we will show that most of the experimental data so far known on the formation of dislocation loops in h.c.p. metals fit fairly well into this concept.

There is one exception: Howe and Rainville [5] reported on TEM investigations on heavy-ion bombarded h.c.p. Co ($c/a < \sqrt{3}$). They interpreted their contrast observations in terms of dislocation loops (of vacancy type) with $\boldsymbol{n} = \{0001\}$ and $\boldsymbol{b} = a/6\,\langle 20\bar{2}3\rangle$, which is in contradiction to the predictions outlined above. Therefore, we have repeated such experiments on h.c.p. Co using 60 keV Au ions for production of the vacancy type loops. In our investigations we make use of some recent developments of the black–white contrast method — presented in [6 to 8] and especially in [9] — which were not known at the time of the investigations of [5].

2. Experimental Details

Single crystalline slices of the required orientation were cut from h.c.p. Co single crystals (electrical resistivity ratio $\varrho(300\text{ K})/\varrho(4\text{ K}) \approx 56$) by spark erosion and subsequently polished by a double jet technique using an electrolyte described by Thieringer and Strunk [10]. The polished specimens (ready for TEM investigation) were irradiated at room temperature with 60 keV Au ions using an ion accelerator described by Häussermann [11]. The ion dose was between 10^{11} and 5×10^{12} ions/cm^2. The irradiated specimens were investigated in a Jeol JEM 150 electron microscope. The microscope was operated at 150 kV. The electron optical magnification was at least 50000.

Transmission foils of three different orientations S were investigated ($\boldsymbol{n}_f$ foil normal):

$$S_1\colon \boldsymbol{n}_f = \{0001\}\,, \qquad S_2\colon \boldsymbol{n}_f = \{11\bar{2}2\}\,, \qquad S_3\colon \boldsymbol{n}_f = \{2\bar{3}10\}\,. \tag{1}$$

Because of the ferromagnetism of the Co specimens (easy direction [0001]) some difficulties arose in connection with maintaining the astigmatism at a sufficiently low level. This was especially true for the specimens S_3.

3. Experimental Results

3.1 Vacancy nature of the loops

A representative dynamical dark field image of a specimen S_1, obtained with $\boldsymbol{g} = \{11\bar{2}0\}$, is shown in Fig. 1. Assigning a black–white vector $\boldsymbol{l}$ (cf. [6 to 9]) to the individual contrast dots it turns out that most of the contrast dots are oriented in such a way that $(\boldsymbol{g} \cdot \boldsymbol{l}) > 0$. A few dots showing $(\boldsymbol{g} \cdot \boldsymbol{l}) < 0$ are in general fairly small and weak in contrast.

A comparison of the effective two-beam extinction length $\xi_g \approx 40$ nm for $\boldsymbol{g} = \{11\bar{2}0\}$ with the mean damage depth $\langle X\rangle = 7$ nm as calculated for a random incidence of 60 keV Au ions on Co [12] allows the conclusion that the defects observable by TEM are almost exclusively located in the first layer L1 of the depth oscillations [6, 8]. Then, since $(\boldsymbol{g} \cdot \boldsymbol{l}) > 0$, it turns out that the defects are of vacancy type.

The few dots showing $(\boldsymbol{g} \cdot \boldsymbol{l}) < 0$ are attributed to loops of vacancy type, too. Their "wrong" sign of $(\boldsymbol{g} \cdot \boldsymbol{l})$ is explained by assuming that they are located deeper inside the foil, i.e. in the layer L2.

3.2 Determination of the loop normal n and the Burgers vector b

3.2.1 Specimen S_1

The specimens S_1 were dynamically imaged using for each specimen at least two of the three essentially different diffraction vectors $\boldsymbol{g} = \{11\bar{2}0\}$. A typical image of this series is shown in Fig. 1. Nearly all of the observed contrast dots can be classified into six groups denotated by A_ν, B_ν, C_ν, $\nu = 1, 2$. The dots characterized by the same

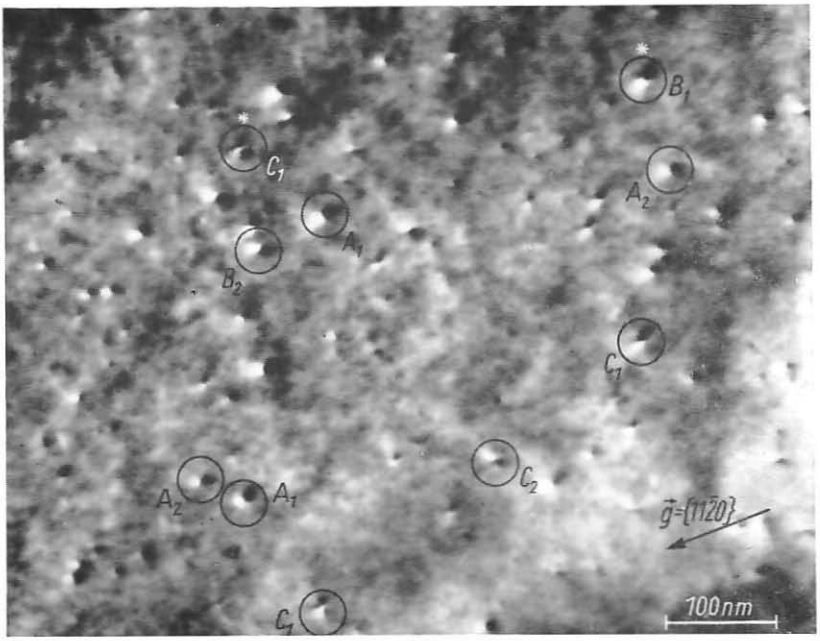

Fig. 1. Dark field micrograph showing black–white contrasts in Co. Foil normal is near {0001}. Typical examples of the A_ν, B_ν, and C_ν contrasts (see text) are encycled. With respect to the asterisks see Fig. 2

capital letter but with different subscripts are related to each other by a mirror operation at a line parallel to $\boldsymbol{g}$. In the notation introduced in [6, 8] the dots A_ν, B_ν, and C_ν may be described as "normal", "slightly distorted", and "strongly distorted" black–white contrast dots, respectively. We have measured the angles φ_l between the positive directions of $\boldsymbol{l}$ and $\boldsymbol{g}$. The result is

$$\varphi_l(A_\nu) = \pm\,(14 \pm 5)^\circ\,, \quad \varphi_l(B_\nu) = \pm\,(35 \pm 5)^\circ\,, \quad \varphi_l(C_\nu) = \pm\,(55 \pm 10)^\circ\,. \quad (2)$$

The $\pm$ in front of the brackets refer to $\nu = 1, 2$, whereas the $\pm$ inside the brackets refer to the experimental scatter. These error limits are, to about equal parts, due to the uncertainty by which the directions of the $\boldsymbol{l}$ vector of an individual contrast dot can be measured and to the differences of the directions of $\boldsymbol{l}$ of the contrast dots of the same group.

So far mainly the following types of Burgers vectors $\boldsymbol{b}$ in h.c.p. metals are discussed in the literature:

$$\boldsymbol{b}_1 = \tfrac{1}{3}\langle 11\bar{2}0\rangle\,, \quad \boldsymbol{b}_2 = \langle 0001\rangle\,, \quad \boldsymbol{b}_3 = \tfrac{1}{3}\langle 11\bar{2}3\rangle\,, \quad \boldsymbol{b}_4 = \tfrac{1}{6}\langle 20\bar{2}3\rangle\,. \quad (3)$$

($\boldsymbol{b}_4$ is a partial Burgers vector). The Burgers vectors $\boldsymbol{b}_2$, $\boldsymbol{b}_3$, and $\boldsymbol{b}_4$ are steeply inclined with respect to the foil plane {0001} of the specimens S_1. Using the criteria for the strength of the black–white contrast as a function of the directions of $\boldsymbol{n}$ and $\boldsymbol{b}$ [6, 8, 9], we conclude that the Burgers vectors $\boldsymbol{b}_2$, $\boldsymbol{b}_3$, and $\boldsymbol{b}_4$ are unlikely to explain the, in general, strong contrast dots visible in Fig. 1. Therefore, we assume

$$\boldsymbol{b} = \boldsymbol{b}_1 = \tfrac{1}{3}\langle 11\bar{2}0\rangle\,. \quad (4)$$

If the loops are of pure edge type, i.e., $\boldsymbol{n}$ parallel to $\boldsymbol{b}_1$, then, by reasons of symmetry, only a threefold variety of types of contrast dots is expected which is in contradiction to the observations, cf. (2). Consequently we assume that the contrast dots are pro-

duced by loops with shear components. Later we will show that there are good arguments that $\boldsymbol{n}$ lies close to $\{10\bar{1}0\}$, with $\sphericalangle(\boldsymbol{n}, \boldsymbol{b}) \approx 30°$. Therefore in the following we start from

$$\boldsymbol{n} = \{10\bar{1}0\}\,, \quad \boldsymbol{b} = \frac{a}{3}\langle 11\bar{2}0\rangle\,, \quad \sphericalangle(\boldsymbol{n}, \boldsymbol{b}) = 30°\,. \tag{5}$$

There are six orientations of loops of this kind. We have calculated for these six orientations the corresponding angles φ_l using the formula presented in [9]. With reference to a particular diffraction vector $\boldsymbol{g} = (11\bar{2}0)$ we obtain

$$\left.\begin{aligned}
&A_1\begin{pmatrix}\boldsymbol{b} = \frac{1}{3}[11\bar{2}0]\\ \boldsymbol{n} = (01\bar{1}0)\end{pmatrix}: \varphi_l(A_1) = +11°; \quad A_2\begin{pmatrix}\boldsymbol{b} = \frac{1}{3}[11\bar{2}0]\\ \boldsymbol{n} = (10\bar{1}0)\end{pmatrix}: \varphi_l(A_2) = -11°\\
&B_1\begin{pmatrix}\boldsymbol{b} = \frac{1}{3}[\bar{1}2\bar{1}0]\\ \boldsymbol{n} = (01\bar{1}0)\end{pmatrix}: \varphi_l(B_1) = +32°; \quad B_2\begin{pmatrix}\boldsymbol{b} = \frac{1}{3}[2\bar{1}\bar{1}0]\\ \boldsymbol{n} = (10\bar{1}0)\end{pmatrix}: \varphi_l(B_2) = -32°\\
&C_1\begin{pmatrix}\boldsymbol{b} = \frac{1}{3}[\bar{1}2\bar{1}0]\\ \boldsymbol{n} = (\bar{1}100)\end{pmatrix}: \varphi_l(C_1) = +51°; \quad C_2\begin{pmatrix}\boldsymbol{b} = \frac{1}{3}[2\bar{1}\bar{1}0]\\ \boldsymbol{n} = (1\bar{1}00)\end{pmatrix}: \varphi_l(C_2) = -51°
\end{aligned}\right\} \tag{6}$$

These calculated values agree excellently with the measured values given in (2).

Taking the error limits in (2) into account we conclude that $\boldsymbol{n}$ may deviate a few degrees ($\lessapprox \pm 5°$) from $\{10\bar{1}0\}$ in direction of $\boldsymbol{b}$ or in the opposite direction. From the experiments presented so far nothing can be said about deviations of $\boldsymbol{n}$ from $\{10\bar{1}0\}$ in directions perpendicular to the basal plane since for the imaging conditions applied for the specimens S_1 the angle φ_l is fairly insensitive to these deviations.

In a next step we have calculated the equal intensity contour diagrams of the six different loop orientations using again a particular $\boldsymbol{g} = (11\bar{2}0)$. The calculations were done using the first order perturbation method [6]. Fig. 2 shows the results for the loop types B_1 and C_1 which should be compared with the corresponding experimental contrast figures of Fig. 1. Taking into account that the constrictions of the equal intensity contour lines at the centres of the contrast figures is an artifact of the approximations of the method [6 to 8] the agreement of the calculated and observed contrast figures is very good. In particular, the calculations reproduce the classification of the observed BW contrast figures into those of "normal" (A_v), "slightly distorted" (B_v) and "strongly distorted" (C_v) shape. A photographic method for the extraction of the equal-intensity contour diagrams from the photographic negatives of the micrographs is briefly described in the Appendix.

Some of the A_v dots of the specimens S_1, especially the larger ones, cf. Fig. 1, show the characteristic fine structure in the centre of the contrast dots which may occur for $|\boldsymbol{g} \cdot \boldsymbol{b}| \gtrapprox 1.5$, cf. [7, 13, 14]. This fine structure was definitely not observed at the B_v or the C_v loops.

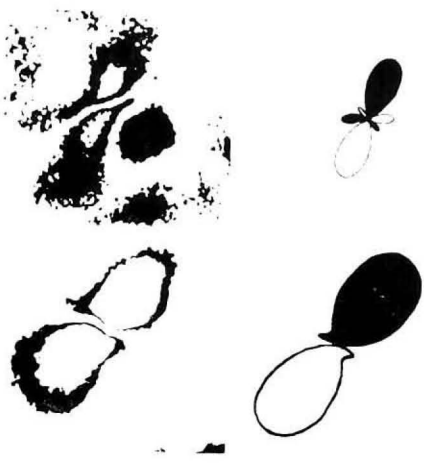

a

b

Fig. 2. Comparison between the a) observed and b) the computed equal intensity contour diagrams of the black–white contrasts. The observed figures are obtained from the black–white contrasts marked with an asterisk in Fig. 1 (upper figures C_1, lower figures B_1)

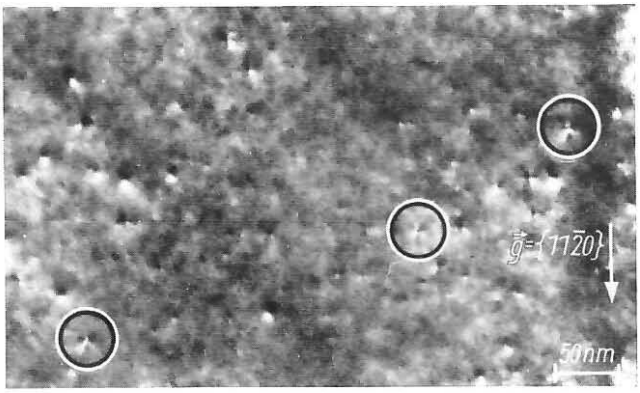

Fig. 3. Dark field micrograph showing "butterfly" contrasts. Foil normal is near {0001}

This result is fully compatible with our indexing; equation (5) gives $(\boldsymbol{g} \cdot \boldsymbol{b}) = \pm 2$ for the A_ν loops and $(\boldsymbol{g} \cdot \boldsymbol{b}) = \pm 1$ for the B_ν and C the$_\nu$ loops.

In the specimens S_1 a few examples (1 to 2%) of the observed contrast dots showed a well developed "butterfly" contrast [6 to 8, 13]. An example is shown in Fig. 3. Contrast dots of butterfly shape are expected if the mean orientation vector $\boldsymbol{m}$ of a loop [8, 9] is perpendicular to $\boldsymbol{g}$ and close to the image plane (= (0001) in the case of S_1)[1]). A number of physically reasonable loop configurations were tested whether they may explain these butterfly contrast dots. However we found only one configuration which explains the observations satisfactorily:

$$\left.\begin{array}{llll} \boldsymbol{n} = \{1\bar{1}00\}\,, & \boldsymbol{b} = \boldsymbol{b}_1 \quad \text{or} & \boldsymbol{b}_2 & \\ \boldsymbol{b}_1 = \frac{1}{2}\langle 1\bar{1}00\rangle\,, & \boldsymbol{b}_2 = \langle 1\bar{1}00\rangle\,, & \boldsymbol{n} \parallel \boldsymbol{b}\,. & \end{array}\right\} \tag{7}$$

In terms of the first-order perturbation method it is difficult to discriminate between $\boldsymbol{b}_1$ and $\boldsymbol{b}_2$. However, a perfect Burgers vector $\boldsymbol{b}_2$ appears unlikely by energetic reasons. Therefore we assume $\boldsymbol{b} = \boldsymbol{b}_1$ (partial Burgers vector).

Assuming equipartition of such loops of pure edge type over the three essentially different directions it follows that only $\frac{1}{3}$ of those loops produce a butterfly contrast, the remaining $\frac{2}{3}$ produce contrasts which could not be distinguished unambiguously, from the contrast of the perfect loops.

3.2.2 Specimen S_2

Dynamical images of the specimens of type S_2 of sufficient quality could only be obtained with one particular diffraction vector of type $\boldsymbol{g} = \{11\bar{2}0\}$. In order to bring this diffraction vector into the exact Bragg position the foil must be tilted by about 30° into an orientation of the image plane given by $\boldsymbol{n}_i \approx \{1\bar{1}01\}$. Fig. 4 shows a micrograph obtained under this condition. All observed contrast dots can be classified as of "normal" shape and can be divided into two groups denoted by A_1' and A_2' which are about symmetrical with respect to a line through $\boldsymbol{g}$ as a mirror line. A measurement of the angle φ_l between $\boldsymbol{l}$ and $\boldsymbol{g}$ yields $\varphi_l(A_\nu') = \pm\,(8 \pm 4)°$.

Here again the error limits within the bars are due to the experimental accuracy and a scatter of the directions of $\boldsymbol{l}$ as well. Assuming as a particular case $\boldsymbol{g} = (11\bar{2}0)$ and $\boldsymbol{n}_i = (1\bar{1}01)$ the observed contrast dots can be explained by the loops of the group A_1 and A_2 as given in (6). Application of the formula for φ_l as presented in [9] gives $\varphi_l(A_\nu') = \pm 6°$ which agrees well to the observed values. In the specimens S_2 the angle

[1]) The vector $\boldsymbol{m}$ is defined as $\boldsymbol{m} = (\boldsymbol{n} \pm \boldsymbol{b})/|\boldsymbol{n} \pm \boldsymbol{b}|$ where the upper (lower) sign holds for loops of vacancy type, characterized by $\boldsymbol{n} \cdot \boldsymbol{b} > 0$ (interstitial type, characterized by $\boldsymbol{n} \cdot \boldsymbol{b} < 0$).

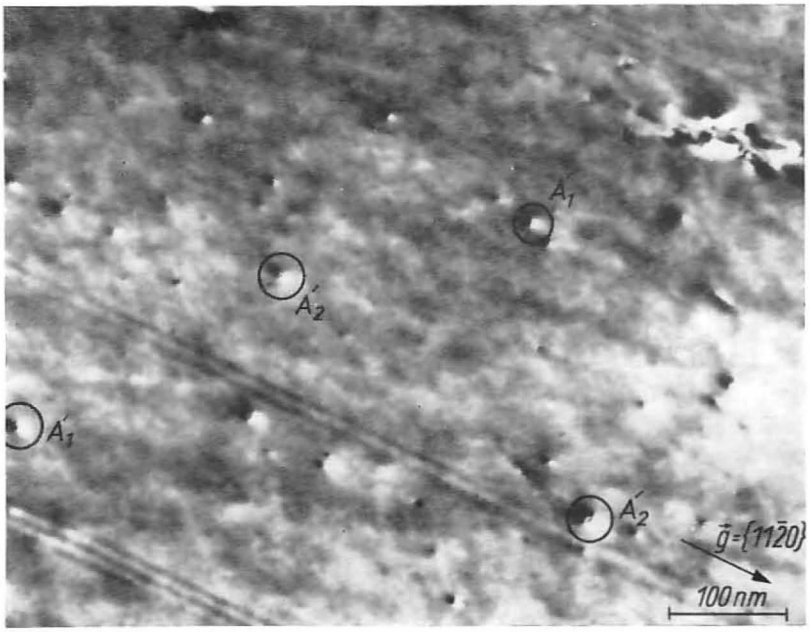

Fig. 4. Dark field micrograph of black–white contrasts in a specimen with foil normal near $\{11\bar{2}2\}$; normal of the image plane near $\{1\bar{1}01\}$

φ_l is sensitive to deviations of $\boldsymbol{n}$ from $\{10\bar{1}0\}$ towards $\{0001\}$. From the scatter of the measured φ_l-values we conclude that this deviation is probably not more than about $\pm 5°$.

Loops of the groups B_ν and C_ν (cf. (6)) were not observed in S_2. This may be due to either of the following reasons:

(i) The visibility of the black–white contrast dot of a given loop decreases with decreasing angle γ between $\boldsymbol{m}$ and the electron beam direction (normal of the image plane) [6 to 9]. For the loops B_ν and C_ν we have $\gamma = 55°$ and $39°$ respectively. According to [8, 9] the B_ν and the C_ν loops are oriented close to and far beyond the limit of visibility, respectively.

(ii) For both groups, B_ν and C_ν, the Burgers vector $\boldsymbol{b}$ is inclined to the foil plane by about 55°. In this case there is strong probability that these loops, once they are formed, may slip out of the foil due to the attractive image force caused by the adjacent specimen surface (Jäger et al. [15, 16].)

3.2.3 Specimen S_3

Specimens of this type were imaged with $\boldsymbol{g} = \{0002\}$. Accordingly we have $\boldsymbol{n}_i \approx \approx \boldsymbol{n}_f = \{2\bar{3}10\}$. In spite of considerable efforts a pronounced background modulation of "wavelength" 2 to 3 nm, which is probably caused by preferential etching during polishing, could not be avoided. Furthermore, because of the ferromagnetism of Co the performance of high-resolution micrographs was extremely difficult. A comparatively good micrograph with $\boldsymbol{g} = \{0002\}$ is shown in Fig. 5. In this micrograph a dislocation running inclined through the foil shows a fairly sharp fine structure indicating that in this particular case the resolution should be adequate in order to detect the black–white contrast dots of loops with diameters $\gtrapprox 3$ nm. However, on this and other micrographs of specimens S_3, no black–white contrast dot of a dislocation loop was found. A possible explanation of this fact will be presented in Section 4.1.

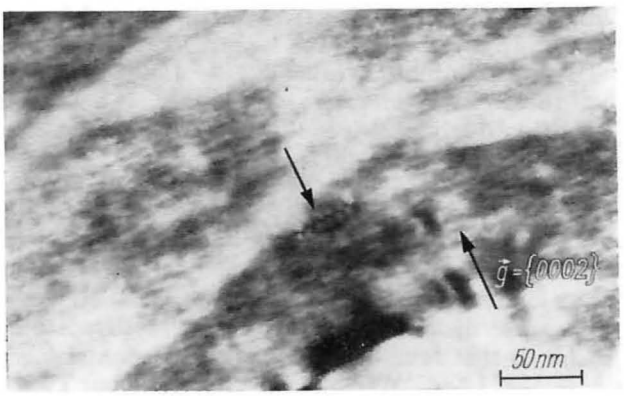

Fig. 5. Dark field micrograph of an irradiated specimen with foil normal near $\{11\bar{2}0\}$. The marked dislocation indicates that the resolution is high enough to detect loops on the {0001} plane with diameters $\geqq 3$ nm

Specimens of type S_3 when imaged with $\boldsymbol{g} = \{0002\}$ are especially suitable in order to detect loops on the basal plane ($\boldsymbol{n} = \{0001\}$) with $\boldsymbol{b} = \frac{1}{6}\langle 20\bar{2}3\rangle$ which were assumed to be present in ion-damaged Co by other authors [5]. Their result is not confirmed in the present investigation.

3.3 Yield factor, size distribution, and clustering efficiency

The yield factor Q is defined as the number of visible defects per incident ion. A typical value for Co is $Q = 0.07$. This value is roughly dose-independent, indicating that each dislocation loop results from the collapse of an individual cascade. The reason for the low value of Q compared to f.c.c. metals is so far unknown.

In order to obtain the size distribution of the loops, the width w of the separation line between the black and the white lobe of the black–white contrasts in specimen S_2 was measured. According to recent results of Katerbau [17], w is almost independent of the depth position of the loop and the best approximation to the real size of the loop. The size distribution obtained in this way is shown in Fig. 6. As a mean diameter $\bar{d}$ we found $\bar{d} = 7$ nm.

The clustering efficiency η_{cl} is defined as the number ν_{L} of vacancies stored in an individual loop divided by the number ν_{C} of vacancies produced in the corresponding cascade. Using the Kinchin-Pease model ν_{C} can be estimated to

$$\nu_{\mathrm{C}} = \frac{E_{\mathrm{i}}}{2E_{\mathrm{d}}} \tag{8}$$

with E_{i} energy of the incident ion and E_{d} displacement energy. Taking $E_{\mathrm{d}} = 22$ eV [18] and inserting $\bar{d}$ for a calculation of ν_{L} we obtain $\eta_{\mathrm{cl}} = 0.56$ which compares well

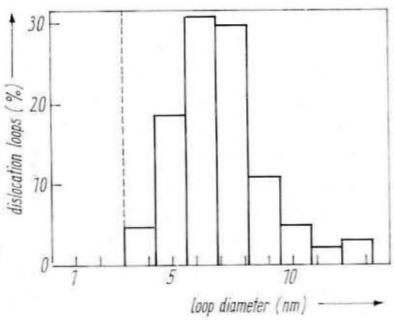

Fig. 6. Size distribution of the black–white contrasts. The dashed line refers to the visibility limit

with the fairly high clustering efficiencies observed in heavy-ion bombarded f.c.c. metals [3]. If, however, the largest loops of the size distribution are used ($d_{\max} \approx$ $\approx$ 12 nm) we obtain a value $\eta_{\max} \approx 1.6 > 1$ which cannot be true, cf. also [2]. Perhaps these "large" loops are not produced in a single cascade event but rather by a collapse of two adjacent loops — of which at least one is glissile — due to their elastic interactions.

4. Discussion

4.1 Model for the formation of vacancy loops in h.c.p. cobalt

In the preceding sections we have shown that damage in Co produced by energetic heavy ion results in the formation of dislocation loops of vacancy type (mean diameter $\approx$ 7 nm) at distances $\lesssim$ 10 nm below the irradiated specimen surface. This result is similar to that found in a number of f.c.c. and b.c.c. metal irradiated under similar conditions [1 to 4]. We were able to explain our TEM observations assuming that most of the vacancy loops have a perfect Burgers vector of type $\boldsymbol{b} = \frac{1}{3}\langle 11\bar{2}0\rangle$ and a plane normal $\boldsymbol{n}$ close to $\{10\bar{1}0\}$ ($\sphericalangle\, \boldsymbol{n}, \boldsymbol{b} \approx 30°$). The deviations of $\boldsymbol{n}$ from this direction was estimated to be $\lesssim 5°$, parallel and perpendicular to the basal plane.

In addition to the perfect loops a small number of "Frank" loops of pure edge type with $\boldsymbol{n} = \{10\bar{1}0\}$ and $\boldsymbol{b} = \frac{1}{2}\langle 10\bar{1}0\rangle$ were identified. In these cases the loop area is faulted with atoms in a head-on position. The specific energy of such a stacking fault is assumed to be fairly high.

The results described above suggest a two-step mechanism of the formation of dislocation loops in h.c.p. metals which was already sketched briefly in Section 1 and which is similar to that outlined in [16] for the case of heavy-ion damage in (b.c.c.) tungsten.

(i) Single point defects (vacancies or interstitials, respectively) agglomerate in a monoatomic layer on a close-packed plane of the type $\boldsymbol{h}_{\text{c.p.}} = \{hkil\}_{\text{c.p.}}$. For $c/a > \sqrt{3}$ we have $\boldsymbol{h}_{\text{c.p.}} = \{0002\}$ whereas in the case of $c/a < \sqrt{3}$ this is true for $\boldsymbol{h}_{\text{c.p.}} = \{1\bar{1}00\}$. Thus in the case of Co ($c/a \approx 1.63$) a pure edge loop with a partial Burgers vector $\boldsymbol{b} = \frac{1}{2}\langle 1\bar{1}00\rangle$ is formed as the first step. Because of the high specific stacking fault energy of the loop area this configuration is energetically favoured only as long as the loops are still fairly small.

(ii) If a loop reaches during its growth a critical size (which is obviously considerably smaller than the observed mean loop diameter $\bar{d} = 7.0$ nm) the stacking fault is eliminated by a shear over the loop area. This transformation may be described for the particular case $\boldsymbol{n} = (10\bar{1}0)$ and $\boldsymbol{b} = \boldsymbol{b}_{\text{e}} = \frac{1}{2}[10\bar{1}0]$ by

$$\left.\begin{aligned} \boldsymbol{b}_{\text{e}} + \boldsymbol{b}_{\text{s}} &= \boldsymbol{b}_{\text{p}} \\ \tfrac{1}{2}[10\bar{1}0] + \tfrac{1}{6}[\bar{1}2\bar{1}0] &= \tfrac{1}{3}[11\bar{2}0]\,, \\ \tfrac{1}{2}[10\bar{1}0] - \tfrac{1}{6}[\bar{1}2\bar{1}0] &= \tfrac{1}{3}[2\bar{1}\bar{1}0]\,. \end{aligned}\right\} \tag{9}$$

(The subscripts e, s, and p refer to "edge", "shear" and "perfect", respectively). As a result of this transformation we obtain loops of that kind which we could assign to most of the observed BW contrast dots.

After transformation the loop may rotate in order to bring the angle ε between $\boldsymbol{b}$ and $\boldsymbol{n}$ into its energetic equilibrium value ε_0 (cf. [19]). For loop sizes as observed in the present experiments and assuming elastic isotropy ε_0 lies in the range between 25° and 35° and may reach even 40° for comparatively small loops. Since we have $\varepsilon = 30°$ directly after the transformation, the approach to the equilibrium needs in general only small rotations of $\boldsymbol{n}$ and this may explain the observed small scatter of the directions of $\boldsymbol{n}$. The shapes of the "strongly distorted" contrast dots as observed in specimens of orientation S_1 (cf. Section 3.2.1) are fairly sensitive to small variations

of ε. In some cases it could be concluded from the shape of the contrast dots (rather than from the direction of the vector $\boldsymbol{l}$) that ε is larger than 30° and close to 40°. The question whether these loops were comparatively small was not investigated.

The shear transformation described by (9) requires the nucleation of a partial dislocation (Burgers vector $\boldsymbol{b}_s$) which must subsequently slip over the loop area. Both, nucleation and slipping, may be prevented by details of the atomistic structure of the loop. Thus it is not surprising that in some cases the transformation was blocked so that we were able to observe and identify loops in the unsheared configuration.

Equation (9) shows that there exist two shear directions which permit to transform the partial Burgers vector of a particular edge loop into a perfect Burgers vector. In the bulk material both shear directions are equivalent. By studying ion damage in tungsten Häussermann [20] and Jäger and Wilkens [16] could show that this may be no longer true if the elastic interaction of the loops with the adjacent specimen surface becomes significant [15]. In this case one of the two shear directions is preferred which leads to the stronger (negative) elastic interaction energy of the loop with the surface and thus to the lower total energy. In practice that shear direction is preferred which results in a larger angle between the resultant Burgers vector $\boldsymbol{b}_p$ and the plane of the adjacent specimen surface. Subsequently, just these loops with the steeper inclination of $\boldsymbol{b}_p$ with respect to the adjacent specimen surface are especially susceptible for a slipping out of the specimen (cf. [16]). This mechanism may help to explain why in specimens of orientation S_3 no loops could be observed: It turns out that, in the notation of (6), the only loop orientation, A_1, which should be visible under the imaging condition applied, may be formed with a strongly reduced probability; e.g. edge loops with $\boldsymbol{n} = (0\bar{1}10)$ may transform preferentially into the loop orientation B_1 rather than into A_1.

Summarizing this section we may state that all experimental observations fit well into the proposed two-step mechanism for the formation of dislocation loops in h.c.p. cobalt.

4.2 Comparison with the results of other authors

4.2.1 Axial ratio $c/a < \sqrt{3}$

In the particular case of h.c.p. Co the results of Howe and Rainville [5] were already mentioned in the introduction. The results of these authors are in contrast to the model given in Section 4.1. However, taking into account the recent developments of the BW contrast method the present authors are sure that the TEM observations of [5] can be explained better in terms of the model of Section 5.1 rather than in terms of the model of [5].

With respect to other h.c.p. metals with $c/a < \sqrt{3}$ we refer to the investigations of Brimhall and Mastel [21] on Re and Bernstein and Gulden [22] and Kelly and Blake [23] on Zr. In both metals, after neutron irradiation and subsequent annealing treatment, interstitial loops were found with $\boldsymbol{b} = \frac{1}{2}\langle 11\bar{2}0\rangle$ and $\boldsymbol{n}$ close to $\boldsymbol{b}$ or, at least, close to $\{1\bar{1}00\}$ ($\sphericalangle\, \boldsymbol{n} \cdot \boldsymbol{b} \lessapprox 30°$). If the possibility for an arrangement of the loop normal $\boldsymbol{n}$ with respect to $\boldsymbol{b}$ after the shear transformation of the faulted loop is taken into account (cf. Section 4.1), these results appear in good accordance with the model of Section 4.1.

Mg seems to play an ambivalent role: Hampshire and Hardie [24] found in quenched Mg dislocation loops of vacancy type on the basal plane — which is in contradiction to the model of Section 4.1. However Hillairet et al. [25] and Levy [26] have shown that in the case of Mg the habit plane of the loops produced by quenching or by neutron-irradiation depends on the impurity content (cf. also Lally and Patridge [27]): In the most pure specimens investigated fairly large loops of nearly edge type (di-

ameter ≈ 100 nm) were found with $\boldsymbol{b} = \frac{1}{2}\langle 11\bar{2}0\rangle$ and $\boldsymbol{n}$ close to $\boldsymbol{b}$. This result is in good accordance with the model of Section 4.1: For loops of such a size the equilibrium angle ε between $\boldsymbol{n}$ and $\boldsymbol{b}$ may be in the order of 10° or even less.

4.2.2 Axial ratio $c/a > \sqrt{3}$

For Zn and Cd, which belong to $c/a > \sqrt{3}$, we expect from the model of Section 4.1 a nucleation of pure edge loops on the basal plane ($\boldsymbol{b} = \frac{1}{2}\langle 0001\rangle$). In the case of vacancy loops this leads to a head-on position of atoms at the loop area which corresponds to a stacking fault of high energy. This head-on position may subsequently be transformed into a stacking fault of fairly low energy by a shear process over the loop area. As a result we expect that vacancy loops in h.c.p. metals with $c/a > \sqrt{3}$ should be formed with $\boldsymbol{n} = \{0001\}$ and with a partial Burgers vector $\boldsymbol{b} = \frac{1}{6}\langle 20\bar{2}3\rangle$. Vacancy loops of this configuration were in fact observed in ion-damaged Cd (Price [28]) and in quenched Zn (Berghezan et al. [29], van Tendeloo et al. [30]).

5. Summary and Conclusions

(i) TEM observations show that the damage produced by 60 keV Au ions in h.c.p. cobalt leads to the formation of small dislocation loops of vacancy type in the cores of the displacement spikes.

(ii) The yield factor Q was found to be ≈ 0.07 which is fairly low as compared to f.c.c. metals.

(iii) Inserting the mean loop diameter $\bar{d} \approx 7$ nm a cascade efficiency $\eta_{\mathrm{cl}} \approx 0.56$ is calculated which agrees well with similarly high values as obtained in heavy-ion bombarded f.c.c. metals.

(iv) Most of the observed loops were successfully interpreted in terms of $\boldsymbol{b} = \frac{1}{2}\langle 11\bar{2}0\rangle$, $\boldsymbol{n} \approx \{1\bar{1}00\}$, $\sphericalangle\, \boldsymbol{n}, \boldsymbol{b} \approx 30°$. A small percentage of the loops were found to be of pure edge type with $\boldsymbol{b} = \frac{1}{2}\langle 1\bar{1}00\rangle$ and $\boldsymbol{n} = \{1\bar{1}00\}$.

(v) The results obtained on h.c.p. Co and corresponding results on the formation of dislocation loops in other radiation damaged or quenched h.c.p. metals reported in the literature are in essential agreement with a two-step model of the formation of dislocation loops which was originally established for the formation of dislocation loops in b.c.c. and f.c.c. metals.

Acknowledgements

The authors are indebted to Dr. M. Rühle and Dipl.-Phys. W. Jäger for their help during the first stage of the experimental work. Thanks are also to Miss M. Rapp and Mrs. I. Klicpera for their assistance in preparing the transmission specimens and performing the photographic work.

Appendix

Extraction of equal intensity contour diagrams from micrographs

For a quantitative evaluation and for a suitable presentation of micrographs an equal intensity contour diagram of a particular contrast figure is often desirable. If no densitometer operating in two dimensions is available, such contour diagrams can be obtained from the negative by use of a special film (Agfacontour). If an original negative is "printed" on this film, it responds to the exposure in the following way: The film is blackened only on sites corresponding to the density interval $d + \Delta d$ on the original negative. The level of d can be controlled by the exposure time t_{ex}, the width Δd by the degree of (yellow) filtering of the light. Varying t_{ex} yields a series of

equal intensity contour diagrams, each diagram at another density level. These levels can be controlled quantitatively by copying simultaneously a grey wedge with the negative. The equal intensity series may be used to obtain diagrams as shown in Fig. 2 or for constructing a very instructive coloured "micrograph"; each colour corresponding to a certain density of the original. The granularity of the original negative leads only to a "jitter" of the contour lines, thus high optical enlargements are possible (as opposed to magnifications of the original where, normally, the granularity prevents high optical enlargements). Therefore such "micrographs" are especially useful for the presentation of small contrast details which are often hard to recognize on copies or slides — especially for persons who are not familiar with electron micrographs. For details the reader is referred to [31].

References

[1] M. Wilkens, in: Vacancies and Interstitials in Metals, Ed. A. Seeger, D. Schumacher, W. Schilling, and J. Diehl, North-Holland Publ. Co., Amsterdam 1969 (p. 485).
[2] M. Wilkens, in: Application of Ion Beams to Metals, Ed. S. T. Picraux, E. P. EerNisse, and F. L. Vook, Plenum Press, New York 1974 (p. 441).
[3] M. Wilkens, in: Fundamental Aspects of Radiation Damage in Metals, Ed. M. T. Robinson and F. W. Young, USERDA, Conf. 751006, 1975 (p. 98).
[4] B. L. Eyre, J. Phys. F **3**, 422 (1973).
[5] L. M. Howe and M. Rainville, phys. stat. sol. (a) **7**, 125 (1971).
[6] M. Wilkens and M. Rühle, phys. stat. sol. (b) **49**, 749 (1972).
[7] F. Häussermann, M. Rühle, and M. Wilkens, phys. stat. sol. (b) **50**, 445 (1972).
[8] M. Wilkens, Proc. Internat. School on Electron Microscopy, Erice 1973, in the press.
[9] M. Wilkens and H. Föll, in preparation.
[10] H.-M. Thieringer and H. Strunk, Z. Metallk. **69**, 584 (1969).
[11] F. Häussermann, Phil. Mag. **25**, 537 (1972).
[12] K. B. Winterbon, P. Sigmund, and J. B. Sanders, Mat. Fys. Medd. Dan. Vid. Selesk. **37**, No. 14 (1970).
[13] B. L. Eyre, in: Defects in Refractory Metals, Ed. R. de Batist, J. Nihoul, and L. Stals, S.C.K./C.E.N. Mol 1972 (p. 311).
[14] K.-H. Katerbau, phys. stat. sol. (a) **38**, 463 (1976).
[15] W. Jäger, M. Rühle, and M. Wilkens, phys. stat. sol. (a) **31**, 525 (1975).
[16] W. Jäger and M. Wilkens, phys. stat. sol. (a) **32**, 89 (1975).
[17] K.-H. Katerbau, unpublished.
[18] F. Maury, P. Vajda, A. Lucasson, P. Lucasson, G. Roux, and C. Minier, Phil. Mag. **22**, 1265 (1970).
[19] P. G. Bacon, R. G. Crockner, in: Lattice Defects in Quenched Metals, Ed. R. M. J. Cotterill, M. Doyama, J. J. Jackson, and M. Meshi, Academic Press 1965 (p. 667).
[20] F. Häussermann, Phil. Mag. **25**, 583 (1972).
[21] J. L. Brimhall and B. Mastel, phys. stat. sol. **27**, K89 (1968).
[22] I. M. Bernstein and T. D. Gulden, Phil. Mag. **14**, 1087 (1966).
[23] P. M. Kelly and R. G. Blake, Phil. Mag. **28**, 415 (1973).
[24] J. M. Hampshire and D. Hardie, Acta metall. **22**, 657 (1974).
[25] J. Hillairet, C. Mairy, J. Espinasse, and V. Levy, Acta metall. **18**, 1285 (1970).
[26] V. Levy, J. Microscopie **19**, 1 (1974).
[27] J. S. Lally and P. G. Patridge, Phil. Mag. **13**, 9 (1966).
[28] P. B. Price, Phys. Rev. Letters **6**, 615 (1961).
[29] A. Berghezan, A. Fourdeux, and S. Amelinckx, Acta metall. **9**, 464 (1961).
[30] G. van Tendeloo, J. van Landuyt, and S. Amelinckx, Crystal Lattice Defects **5**, 207 (1974).
[31] E. Ranz, Visual **8**, 49 (1970).

(Received December 6, 1976)